STRAIN RATE FIELDS OVER CAMPBELL GLACIER IN EAST ANTARCTICA OBSERVED BY COSMO-SKYMED DIFFERENTIAL SAR INTERFEROMETRY

Hyangsun Han and Hoonyol Lee*

Department of Geophysics, Kangwon National University, Republic of Korea
hyangsun@kangwon.ac.kr, hoonyol@kangwon.ac.kr*

ABSTRACT ... In this study, we measured strain rate fields over Campbell Glacier (CG) in East Antarctica from 14 COSMO-SkyMed one-day tandem differential interferometric SAR (DInSAR) image pairs obtained from January to November 2011. We removed signals of the vertical tidal deflection of Campbell Glacier Tongue (CGT), a seaward extension of CG, from the DInSAR signals by using tide deflection ratio and tidal variations predicted by Ross_Inv tide model. A map of mean ice-flow velocity along flow lines was generated from the one-day ice flows extracted from the 14 DInSAR dataset. We calculated the longitudinal, transverse, shear, and vertical strain rate from the ice-flow velocity. By analyzing the strain rates, we confirmed that the transverse crevasses form due to the longitudinal extension of ice, while the longitudinal crevasses form due to the divergence of ice-flow and dissipate by the convergence of ice-flow. The western side of CG and the branch stream of CGT showed high shear strain due to lateral drag of ice. The negative vertical strain rates were observed over the grounded part of CG, which represents ice thinning by the seaward ice-flow.

KEY WORDS: Campbell Glacier, Campbell Glacier Tongue, Strain rate, Ice-flow velocity, COSMO-SkyMed, DInSAR

1. INTRODUCTION

Strain rate over a glacier are critical to understanding ice dynamics such as glacier flow regime and crevasse formation (Harper et al., 1998). The strain rate can be derived from ice-flow velocity fields, which can be measured by synthetic aperture radar (SAR) that is powerful tool to observe polar glaciers because it is all-weather and day-and-night imaging system. Differential Interferometric SAR (DInSAR) technique provides surface displacement with centimeter accuracy, which has been used to map ice-flow velocity over a glacier.

A floating glacier such as ice shelf or ice tongue, a seaward extension of an outlet glacier, experiences the vertical tidal deflection due to ocean tide and gravitational ice flow in the horizontal direction as well. As a result, DInSAR signals over the floating glacier contain displacement components of both the ice-flow and the tidal deflection during the interferometric data acquisitions (Rignot et al., 2011a). Therefore, the vertical tidal deflection should be cancelled out from the DInSAR signals to measure accurate ice-flow velocity of the floating glaciers. However, few studies corrected the effect of tidal deflection on the DInSAR-derived ice-flow velocity of floating glaciers.

Several studies corrected tidal effect on ice-flow velocity by removing the amount of tidal variation predicted by tide models from DInSAR signals over floating glaciers (Rignot et al., 2011b; Scheuchl et al., 2012). However, they performed tidal effect correction for a few ice shelves and ignored the spatial variation of tidal response in hinge zone of the ice shelves.

The vertical tidal deflection of a floating glacier can be found by double-differential interferometric SAR (DDInSAR) technique that differentiates two DInSAR signals by assuming that ice-flow is steady during the DInSAR observations (Rignot, 2011a). The ratio of the vertical tidal deflection over tide height, defined as tide deflection ratio (α), can be determined by comparing the DDInSAR-derived tidal deflection of ice with tidal variation during the DDInSAR observations (Han and Lee, 2014). The α values enable the estimation of the spatial variation of the vertical tidal deflection for any tide height and the extraction of accurate ice-flow velocity from DInSAR data.

In this study, we measure ice-flow velocity over Campbell Glacier (CG) in East Antarctica from 14 COSMO-SkyMed one-day tandem DInSAR pairs to derive strain rate fields over the glacier. We remove signals of the vertical tidal deflection over Campbell Glacier Tongue (CGT), a seaward extension of CG, from the DInSAR signals by using the map of α over CGT (Han and Lee 2014). Strain rate fields of CG and CGT are derived from the DInSAR-measured ice-flow velocity, from which we analyze ice-flow regime and formation of crevasses.

2. STUDY AREA AND DATA

CG originated from the end of Mesa Range in Victoria Land in East Antarctica, is a fast-flowing outlet glacier with length of about 110 km. CG flows into the northern Terra Nova Bay in Ross Sea and forms CGT which is composed of two ice streams: one is the main stream and the other is the branch stream (Fig. 1). The white dotted lines in Fig. 1 represent the grounding line location of CGT (Han and Lee, 2014). Many crevasses exist on surface of CG and CGT. Representative crevasse zones

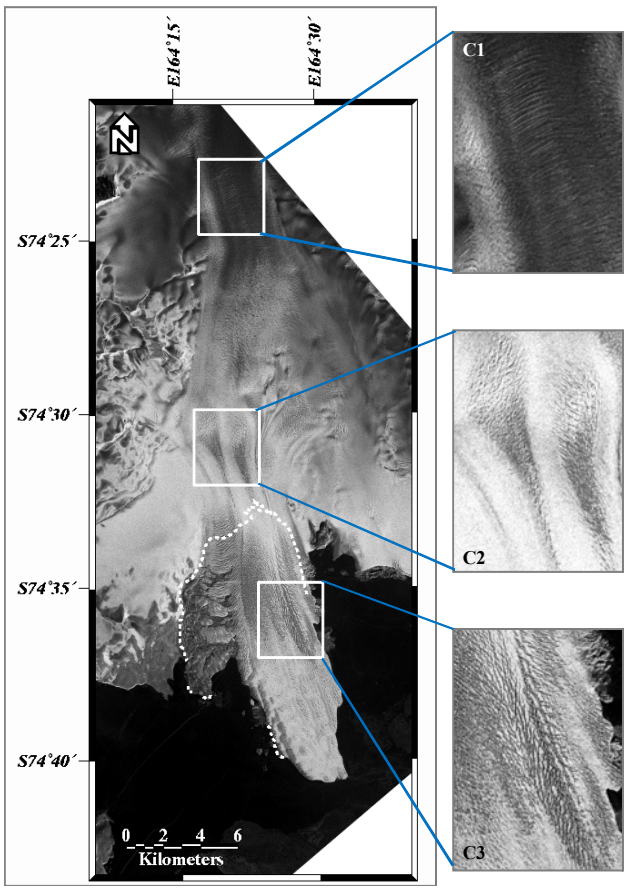

Fig. 1. COSMO-SkyMed SAR image over Campbell Glacier obtained on 27 November 2011.

are indicated as white boxes in Fig. 1. The crevasses on the uppermost part of CG, shown as box C1 in Fig. 1, are formed across the glacial flow line. A white dotted line in box C1 is a transect line parallel to ice-flow line, from which profile of longitudinal strain rate will be analyzed in Section 4. In box C2 and C3, many crevasses form semi-parallel to the glacier flow. In this paper, we analyze the formation of the crevasses for the crevasse zones of C1, C2 and C3 by interpreting the strain rate fields.

We use 14 one-day tandem DInSAR image pairs over CG and CGT obtained from January to November 2011 by COSMO-SkyMed satellites equipped with X-band SAR (Table 1). We also use two COSMO-SkyMed SAR images obtained on 17 October and 2 November 2011 to estimate ice-flow direction by performing the offset tracking method. All the SAR images were acquired with 1 m resolution in strip-map mode, incidence angle of 40°, VV-polarization, and in descending orbit at around 3:45 UTC. ASTER GDEM is used to remove topographic phases from the COSMO-SkyMed interferograms.

Ross_Inv tide model is used to predict tide height at a center point on CGT beyond hinge zone. The effect of load tide is corrected by using TPXO6.2 Load Tide model. The inverse barometer effect (IBE), ~1.01 cm change in tide height per 1 mbar change in atmospheric pressure, of the predicted tide height is corrected by

Table 1. COSMO-SkyMed one-day tandem DInSAR pairs used in this study.

Dates	Perp. Baseline (m)	Height ambiguity (m)	Tidal variation (cm)
2011/01/26,2011/01/27	18.9	424.7	-11.6
2011/02/27,2011/02/28	5.7	1407.2	-4.5
2011/03/15,2011/03/16	-44.4	180.8	-17.5
2011/03/31,2011/04/01	-39.2	204.9	8.3
2011/05/02,2011/05/03	-89.6	89.7	8.3
2011/05/18,2011/05/19	75.9	105.9	27.8
2011/06/03,2011/06/04	-36.5	220.3	-3.3
2011/06/19,2011/06/20	-47.5	169.1	-14.7
2011/08/22,2011/08/23	181.7	44.2	27.6
2011/09/07,2011/09/08	37.3	215.2	1.0
2011/10/09,2011/10/10	-44.4	181.2	5.8
2011/10/25,2011/10/26	-110.9	72.4	-14.0
2011/11/10,2011/11/11	-91.7	87.6	2.0
2011/11/26,2011/11/27	-23.4	342.8	7.5

using in situ atmospheric pressure measured by the AWS installed near CGT from 2010 to 2012.

We also use the map of α (α-map) of CGT, which was generated by performing linear regression analysis between the DDInSAR-derived tidal deflection and tidal variations predicted by the IBE-corrected Ross_Inv (Han and Lee, 2014).

3. METHOD

First, we generate 14 one-day tandem differential interferograms by performing 2-pass DInSAR technique. The vertical accuracy of the ASTER GDEM (20 m) is enough to remove topographic phases from the COSMO-SkyMed interferograms due to very short perpendicular baselines of the one-day tandem DInSAR pairs (Table 1).

DInSAR signals of an ice tongue (ϕ_{LOS}) is the sum of the horizontal ice-flow (ϕ_{LOS}^{flow}), the vertical tidal deflection (ϕ_{LOS}^{tide}) and DInSAR phase errors projected in the line-of-sight (LOS) direction. To account for ϕ_{LOS}^{tide}, we use α, defined as the ratio of the vertical tidal deflection of ice over tide height (T). For one-day DInSAR signals, the difference of the ice shelf elevation is related to one-day difference of T, defined here as $\dot{T}$. Therefore, ϕ_{LOS}^{tide} in one-day DInSAR signals can be obtained by

$$\phi_{LOS}^{tide} = \alpha \dot{T} \cos\theta \qquad (1)$$

where θ is radar look angle. By removing ϕ_{LOS}^{tide} from ϕ_{LOS}, we can estimate ϕ_{LOS}^{flow} of floating glacier.

The ϕ_{LOS}^{flow} represents ice-flow in the LOS direction, but it is not in actual flow direction. To determine ice-flow

direction of CG and CGT, we perform the offset tracking between the COSMO-SkyMed SAR images obtained on 17 October and 2 November 2011. Surface displacement of CG and CGT in the range and azimuth direction during the 16 days is estimated from the offset fields, from which we determine the ice-flow direction. By assuming that ice-flow direction is unchanged with time, we convert the ice-flow in the LOS direction derived from the DInSAR images to that in the ice-flow direction estimated by the offset tracking results. We then generate the map of the average ice-flow velocity and its standard deviation from the 14 DInSAR-derived one-day ice-flows to represent annual state of the ice-flow.

We calculate strain rates with respect to the image-axes x and y directions, $\dot{\varepsilon}_{xx}$, $\dot{\varepsilon}_{yy}$ and $\dot{\varepsilon}_{xy}$, from the v-map (Harper et al., 1998). We then calculated the flow-oriented strain rates such as longitudinal strain rate $\dot{\varepsilon}_l$, transverse strain rate $\dot{\varepsilon}_t$ and shear strain rate $\dot{\varepsilon}_s$ by using the following equations (Bindschadler et al., 1996):

$$\begin{aligned}\dot{\varepsilon}_l &= \dot{\varepsilon}_{xx}\cos^2\beta + 2\dot{\varepsilon}_{xy}\sin\beta\cos\beta + \dot{\varepsilon}_{yy}\sin^2\beta \\ \dot{\varepsilon}_t &= \dot{\varepsilon}_{xx}\sin^2\beta - 2\dot{\varepsilon}_{xy}\sin\beta\cos\beta + \dot{\varepsilon}_{yy}\cos^2\beta \\ \dot{\varepsilon}_s &= \left(\dot{\varepsilon}_{yy} - \dot{\varepsilon}_{xx}\right)\sin\beta\cos\beta + \dot{\varepsilon}_{xy}\left(\cos^2\beta - \sin^2\beta\right)\end{aligned} \quad (2)$$

where β is the flow direction measured counter-clockwise from the x axis. Assuming that the grounded ice is in an unchanging state, the divergence of the ice-flow velocity is to be zero by applying the continuity condition and we can derive the vertical strain rate $\dot{\varepsilon}_z$ as follows (Bindschadler et al., 1996).

$$\dot{\varepsilon}_z = -\dot{\varepsilon}_l - \dot{\varepsilon}_t \quad (3)$$

The $\dot{\varepsilon}_z$ represents the vertical strain rate at the ice surface only. Nevertheless, the $\dot{\varepsilon}_z$ calculated from the equation (3) can be used as the depth-averaged vertical strain rate due to the vertical change in ice-flow velocity is very low in ice streams (Bindschadler et al., 1996).

4. RESULT AND DISCUSSION

Ice-flow in the LOS direction over CG and CGT was measured from the 14 DInSAR images and that was converted to that in the ice-flow direction estimated by the offset tracking method. We then generated the map of the average ice-flow velocity and its standard deviation. The ice-flow velocity increases from the upper grounded part of CG (~20 cm day^{-1}) to the seaward edge of CGT (~67 cm day^{-1}), and that increases from the glacial margin to the central flow line of the glacier (not shown in this paper). Most areas of CG and CGT show small σ_v less than 4 cm day^{-1} (not shown in this paper), which confirmed that ice-flow velocity was steady during the DInSAR observations. However, some regions show σ_v values larger than 10 cm day^{-1}. Large angle between the LOS and the ice-flow direction might be a reasonable source of the large σ_v value. This is because InSAR observes the phase differences due to the range changes. Therefore, we masked the pixels of the v-map of which the angle between the ice-flow line and the LOS is in [70°, 110°] and then calculated the strain rate fields.

Maps of $\dot{\varepsilon}_l$, $\dot{\varepsilon}_t$, $\dot{\varepsilon}_s$ and $\dot{\varepsilon}_z$ are shown as Fig. 2(a), (b), (c) and (d), respectively. The white dotted lines in Fig. 2 represent the location of grounding line of CGT. All the strain rates have a wide variation on the uppermost grounded part of CG because the ice-flow velocity increases and decreases locally. The $\dot{\varepsilon}_l$-map shows the zones of compression and tension on the glacial surface

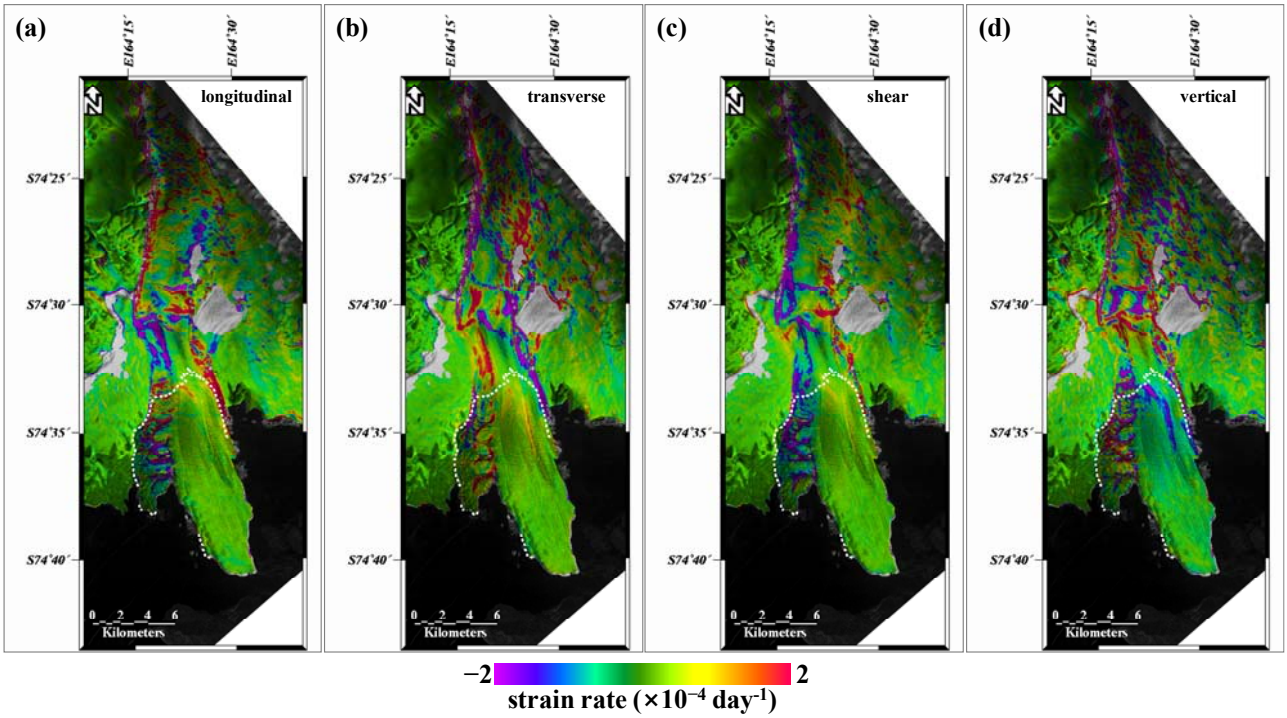

Fig. 2. (a) Longitudinal, (b) transverse, (c) shear, and (d) vertical strain rate over Campbell Glacier.

(Fig. 2a). The $\dot{\varepsilon}_l$ values along the transect line, indicated as the white dotted line in box C1 in Fig. 1, show a mean value of 8×10^{-5} day^{-1}, from which we confirmed that the transverse crevasses were formed by the longitudinal tensile strain. Over the main stream of CGT, $\dot{\varepsilon}_l$ values have a mean of only 1×10^{-5} day^{-1}, which means that there is little change in the flow velocity along flow line.

Map of $\dot{\varepsilon}_t$ shows the zones of convergence and divergence of the ice-flow (Fig. 2b). In the region between 5 km and 7 km upstream of the grounding line (crevasse zone C2 in Fig. 1), $\dot{\varepsilon}_t$ values of $\sim3\times10^{-4}$ day^{-1} are observed near the glacial margin, where the ice-flow diverges due to the widening of glacier width and the longitudinal crevasses form. Ice converges into the region between 3 km and 5 km upstream of the grounding line as the width of glacier narrows, resulting in negative $\dot{\varepsilon}_t$ values of $\sim-3\times10^{-4}$ day^{-1}. The longitudinal crevasses disappear at the zone of ice-flow convergence. The positive $\dot{\varepsilon}_t$ values of $\sim1\times10^{-4}$ day^{-1} are observed in the longitudinal crevasses zone in the main stream of CGT, indicated as box C3 in Fig. 1, which is due to the divergence of ice. The eastern part of the main stream of CGT is grounded (Han and Lee, 2014), of which the ice-flow velocity slows down due to basal drag. Meanwhile, the ice-flow of other regions of CGT increases as distance from the grounding line increases because the effect of basal drag decreases. This is the primary cause of the divergence of the ice-flow and the formation of the longitudinal crevasses on the glacier tongue.

The $\dot{\varepsilon}_s$-map, clearly illustrates the glacier shear margin (Fig. 2c). High negative $\dot{\varepsilon}_s$ values of $\sim-3\times10^{-4}$ day^{-1} are observed along the western sides of the grounded part of CG and the branch stream of CGT due to lateral drag. Most areas of the main stream of CGT shows the $\dot{\varepsilon}_s$ values close to zero due to the absence of the glacial margin channel. In the longitudinal crevasse zone of the main stream of CGT, however, $\dot{\varepsilon}_s$ values are calculated to be $\sim7\times10^{-5}$ day^{-1}. This is due to the rotation of ice which is affected by the geometry of grounding line.

Map of $\dot{\varepsilon}_z$ is shown in Fig. 2(d). The negative $\dot{\varepsilon}_z$ values are dominant on the grounded ice stream, which implies that the ice thinning due to seaward ice-flow of the glacier (Bindschadler et al., 1996). However, the convergence zone of the grounded part of CG, the 5 km upstream of the grounding line, shows high positive $\dot{\varepsilon}_z$ values of $\sim4\times10^{-4}$ day^{-1}, which represents ice thickening by the convergence of the ice-flow. The wide variations in the $\dot{\varepsilon}_l$, $\dot{\varepsilon}_t$, $\dot{\varepsilon}_s$ and $\dot{\varepsilon}_z$ values on the branch stream of CGT are caused by the irregular ice-flow of the broken ice chunks (Han and Lee, 2014).

5. CONCLUSION

We measured strain rate over CG and CGT from accurate ice-flow velocity fields derived from the 14 one-day tandem COSMO-SkyMed DInSAR pairs. The vertical tidal deflection of CGT was estimated by multiplying the one-day difference of tide height predicted by the IBE-corrected Ross_Inv tide model by the DDInSAR-derived tide deflection ratio.

The ice-flow regime and crevasse formation of CG and CGT were analyzed from the flow-oriented and the vertical strain rate fields. The transverse crevasses were formed by longitudinal extension, while the longitudinal crevasses formed at the ice divergence zone and disappeared at ice convergence zone. The western side of CG and the branch stream of CGT experiences lateral drag. Most of ice on the grounded part of CG thinned due to the seaward ice-flow. However, the ice thickened at 5 km upstream of the grounding line by the convergence of the ice-flow.

This study showed that the vertical tidal deflection of a floating glacier must be removed from DInSAR signals to measure accurate ice-flow velocity and strain rate field. The strain rate of ice shelves and ice tongues calculated from tidal-effect corrected ice-flow velocity will be of great value in understating ice dynamics of floating glaciers in more detail.

ACKNOWLEDGMENTS

This work was supported by Basic Science Research Program through the National Research Foundation of Korea (NRF) funded by the Ministry of Education (NRF-2013R1A1A2008062) and also by Space Core Technology Development Program through the NRF funded by the Ministry of Science, ICT and Future Planning (NRF-2013M1A3A3A02041853).

REFERENCES

Bindschadler, R., P. Vornberger, D. Blankenship, T. Scambos, and R. Jacobel, 1996. Surface velocity and mass balance of Ice Streams D and E, West Antarctica. *Journal of Glaciology*, 42(142), pp. 461–475.

Han, H., and H. Lee, 2014. Tide deflection of Campbell Glacier Tongue, Antarctica, analyzed by double-differential SAR interferometry and finite element method. *Remote Sensing of Environment*, 141, pp. 201–213.

Harper, J.T., N.F. Humphrey, and W.T. Pfeffer, 1998. Crevasse patterns and the strain-rate tensor: a high-resolution comparison. *Journal of Glaciology*, 44(146), pp. 68–76.

Rignot, E., J. Mouginot, and B. Scheuchl, 2011a. Antarctic grounding line mapping from differential satellite radar interferometry. *Geophysical Research Letters*, 38, L10504.

Rignot, E., J. Mouginot, and B. Scheuchl, 2011b. Ice flow of the Antarctic Ice Sheet. *Science*, 333(6048), pp. 1427–1430.

Scheuchl, B., J. Mouginot, and E. Rignot, 2012. Ice velocity changes in the Ross and Ronne sectors observed using satellite radar data from 1997 and 2009. *The Cryosphere*, 6, pp. 1019–1030.